Structure of the Bcr-Abl oncoprotein oligomerization domain

Xun Zhao[1], Saghi Ghaffari[2], Harvey Lodish[2], Vladimir N. Malashkevich[1] and Peter S. Kim[1,3]

[1]Howard Hughes Medical Institute, Whitehead Institute for Biomedical Research, Department of Biology, Massachusetts Institute of Technology, Nine Cambridge Center, Cambridge, Massachusetts 02142-1401, USA. [2]Whitehead Institute for Biomedical Research, Department of Biology, Massachusetts Institute of Technology, Nine Cambridge Center, Cambridge, Massachusetts 02142-1401, USA. [3]Present address: Merck Research Laboratories, 770 Sumneytown Pike, West Point, Pennsylvania 19486-0004, USA.

Published online: 7 January 2002, DOI: 10.1038/nsb747

The Bcr-Abl oncoprotein is responsible for a wide range of human leukemias, including most cases of Philadelphia chromosome-positive chronic myelogenous leukemia. Oligomerization of Bcr-Abl is essential for oncogenicity. We determined the crystal structure of the N-terminal oligomerization domain of Bcr-Abl (residues 1–72 or $Bcr_{1–72}$) and found a novel mode of oligomer formation. Two N-shaped monomers dimerize by swapping N-terminal helices and by forming an antiparallel coiled coil between C-terminal helices. Two dimers then stack onto each other to form a tetramer. The $Bcr_{1–72}$ structure provides a basis for the design of inhibitors of Bcr-Abl transforming activity by disrupting Bcr-Abl oligomerization.

The *Bcr-Abl* oncogene is essential in the development of over 95% of chronic myelogenous leukemias (CML) and 20% of acute lymphoblastic leukemias (ALL)[1,2]. *Bcr-Abl* is formed by the fusion of the *Bcr* gene on chromosome 22 with the protooncogene *c-Abl* on chromosome 9 in a reciprocal translocation event that results in the formation of the 'Philadelphia chromosome'[2]. *c-Abl* encodes a nonreceptor tyrosine kinase, whose activity is tightly regulated in normal cells[3]. The fusion of Bcr sequences upstream of *c-Abl* constitutively activates Abl tyrosine kinase and is essential for Bcr-Abl transformation[4,5] (Fig. 1). The N-terminal oligomerization domain of Bcr is required for Abl kinase activation[6]. Therefore, disrupting Bcr oligomerization represents a potential therapeutic strategy for inhibiting Bcr-Abl oncogenicity.

To reveal the molecular details of Bcr-Abl oligomerization and to provide a structural basis for inhibitor design, we expressed, characterized and determined the X-ray crystal structure of the oligomerization domain of Bcr-Abl (residues 1–72 or $Bcr_{1–72}$) (Fig. 1). Initially, we characterized several variants of the oligomerization domain. Previous studies indicated a coiled-coil region for residues 28–68 (ref. 6); therefore, we tested whether this region was sufficient for oligomerization. The coiled-coil segment (residues 30–65 or $Bcr_{30–65}$) (Fig. 1), produced by standard peptide synthesis, formed a stable α-helical structure with a midpoint of thermal denaturation (T_m) of 60 °C. However, $Bcr_{30–65}$ had poor solubility in physiological buffers. We found that residues beyond the coiled-coil segment provided additional structural stability and solubility. The recombinant $Bcr_{1–72}$ formed a stable α-helical structure with a T_m of 84 °C.

Overall architecture of $Bcr_{1–72}$

Diffraction-quality crystals were obtained only when we mutated Cys 38 to Ala in $Bcr_{1–72}$ (denoted $Bcr_{1–72}$C38A). Numerous studies indicated that the structural heterogeneity caused by random oxidation of sulfhydril groups and subsequent protein misfolding often prevents crystallization. $Bcr_{1–72}$C38A demonstrates the same helicity and T_m as $Bcr_{1–72}$. We solved the X-ray crystal structure by using multiwavelength anomalous diffraction (MAD)[7] data from a selenomethionine (SeMet)-substituted $Bcr_{1–72}$ crystal and refined the structure to 2.2 Å resolution (Table 1). The asymmetric unit of the $Bcr_{1–72}$ crystals contains eight equivalent protein chains that form two identical tetramers. This observation is consistent with previous biochemical studies, where tetramers were found for both the oligomerization domain and the full-length Bcr-Abl[6,8]. Each monomer consists of a short N-terminal helix (residues 5–15, referred to as α1), a flexible loop (residues 16–27) and a long C-terminal helix (residues 28–67, referred to as α2) (Fig. 1). Together these form an N-shaped structure, with the loop allow-

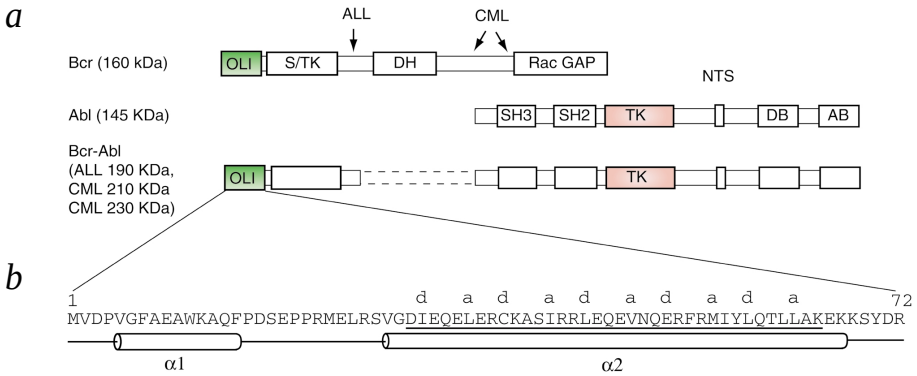

Fig. 1 Structural and functional domains of Bcr, Abl and Bcr-Abl[37]. ***a***, The human Bcr protein contains 1,271 amino acids and multiple domains, including the oligomerization domain (OLI), the serine/threonine kinase domain (S/TK), the domain homologous to the human Dbl and yeast Cdc24 proteins (DH) and the domain with GTPase-activating activity for Rac (RacGAP). The c-Abl protein contains 1,097 amino acids, which include the Src-homology domains 3/2 (SH3/SH2), tyrosine kinase domain (TK), nuclear translocalization signal (NTS), DNA binding domain (DB) and actin-binding motif (AB). Two domains essential for transforming activity — OLI from Bcr and TK from Abl — are depicted in green and red, respectively. The other domains are not colored. Depending on the site of the breakpoint in the *Bcr* gene, the fusion protein can vary in size from 190 to 230 kDa. Each fusion protein contains the same portion of the c-Abl protein but differs in the length of the Bcr portion. The breakpoints in *Bcr* that occur in CML and ALL are indicated by arrowheads. ***b***, The sequence of $Bcr_{1–72}$ is indicated, with the sequence of the coiled-coil region ($Bcr_{30–65}$) underlined. Letters immediately above the sequence indicate the heptad repeat 'a' and 'd' positions. Heptad repeats — a repeated seven-amino acid pattern, denoted $(a–g)_n$, with hydrophobic residues at the first (a) and fourth (d) positions — are a key feature of coiled-coil sequences[38–40]. Cylinders below the sequence indicate the α1 helix (residues 5–15) and the α2 helix (residues 28–67) observed in the crystal structure.

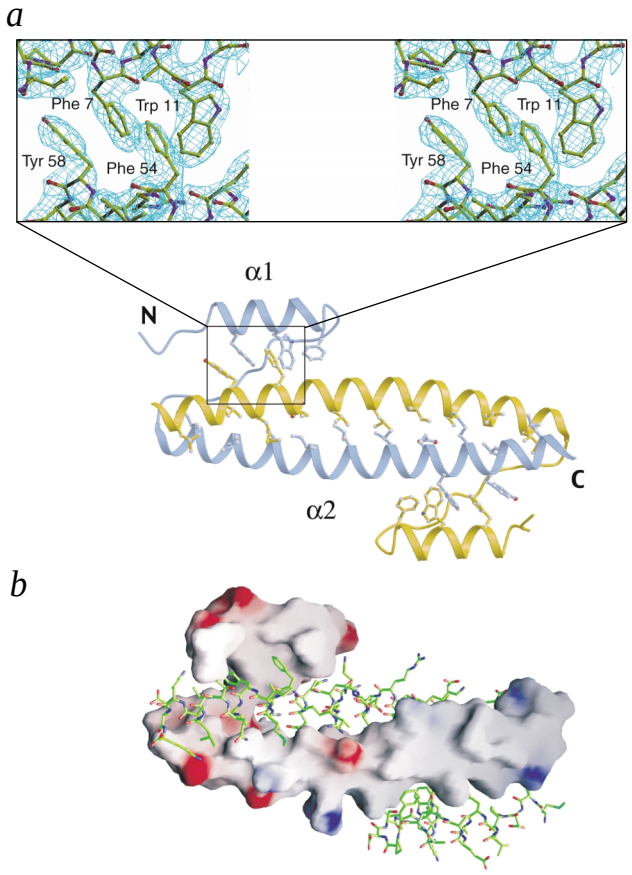

Fig. 2 Extensive interactions in the dimer interface. ***a***, In the dimer, the α2 helix of one monomer (blue) is sandwiched between the α1 and α2 helices of a second monomer (yellow), and *vice versa*. The side chains of 'a' and 'd' residues in the coiled coil and the residues in the aromatic core are displayed. The residues in the coiled-coil region and the aromatic core are well defined in electron density maps (average main chain B-factor ~30 Å^2), whereas residues beyond the interface area and those from the loop are quite flexible (average main chain B-factor ~53 Å^2). The aromatic core is boxed. Inset shows an expanded stereo view of the MAD-phased electron density contoured at 1.2 σ in the area of the aromatic core. For a clearer view, Phe 15 is not shown. ***b***, Surface electrostatic potential of one monomer, with its dimeric partner shown in green. Basic regions are blue, and acidic regions are red. Nearly 4,200 Å^2 of the solvent-accessible surface is buried upon dimer formation. Figure prepared using MOLSCRIPT[41] and GRASP[42].

ing the two helices of one monomer to assume a parallel orientation (Fig. 2*a*).

Dimer interface

The monomers associate into a dimer through the formation of an antiparallel coiled coil between the α2 helices and domain swapping[9] (an exchange of secondary structural elements between constituent monomers) of two α1 helices, where one α1 helix swings back and packs against the α2 helix from the second monomer (Fig. 2*a*,*b*). The four helices in the dimer lie approximately in one plane. The intertwined packing arrangement gives rise to an extensive dimer interface, with a total of 217 van der Waals contacts (radius cutoff = 4 Å), seven salt bridges and three hydrogen bonds.

More than half of the dimer interface lies within the hydrophobic core in the antiparallel coiled coil. Most of the residues at 'a' and 'd' positions of the heptad repeat (Fig. 1) — including Ile 31, Leu 35, Ile 42, Leu 45, Val 49, Met 56, Leu 59 and Leu 63 — are hydrophobic and pack in a typical 'knobs-in-holes' mode[10,11]. The exception is Glu 52 at position 'd'; this charged residue is stabilized by forming an intrachain salt bridge with Arg 55 at position 'g'. Apart from the hydrophobic core in the coiled-coil interface, there is a predominantly aromatic core between the α1 helix of one chain (including Phe 7, Trp 11 and Phe 15) and the α2 helix of the other chain (including Phe 54 and Tyr 58) (Fig. 2*a*, inset). This exchange of α1 helices buries a hydrophobic patch on the outer surface of the coiled coil and provides additional structural stability. Our structure reveals an efficient way of assembling dimers and providing improved stability by using a hybrid of two distinct oligomerization modes — antiparallel coiled-coil packing and domain swapping — that are both recognized as important mechanisms for forming oligomeric proteins[9,12].

Tetramer *versus* dimer in kinase activation

Two dimers associate into a tetramer with an ~130° crossing angle between the dimer coiled-coil axes (Fig. 3); notably, the dimer–dimer interface is significantly less polar than the solvent-exposed surface (Fig. 4). However, the physiological significance of tetramer formation remains to be determined. Previous studies have shown that substitution of the Bcr oligomerization domain with the GCN4 dimeric, parallel coiled coil also activated kinase activity[13]. In addition, different dimerization motifs, such as the helix-loop-helix domain in Tel oncoprotein, can activate Abl and lead to a different type of leukemia[14]. These results support the notion that the mere clustering of kinase domains, mediated by dimerization, is sufficient to induce activation in a way similar to the activation of receptor tyrosine kinases by ligands[15]. However, our crystal structure suggests that a tetramer might be more efficient than a dimer in bringing downstream domains together. The distance between the two C-termini in the dimer is ~60 Å, whereas tetramer formation brings opposite C-termini across the dimer–dimer interface into a closer proximity of ~24 Å. An interesting test of whether tetramerization further potentiates the Abl tyrosine kinase activity induced by a dimer alone would be to disrupt the dimer–dimer interface.

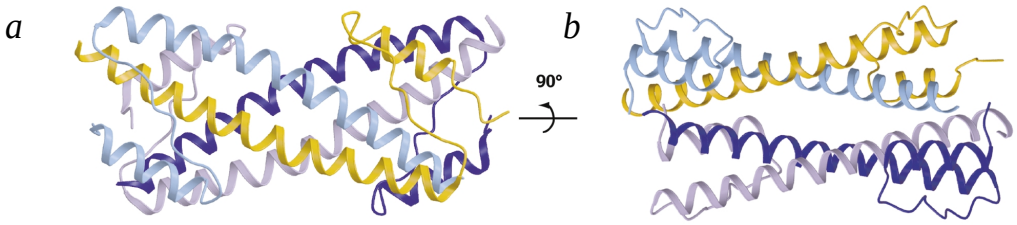

Fig. 3 Packing of Bcr$_{1–72}$ tetramers with two orthogonal views. The tetramer has an approximate 222-point symmetry, with three two-fold rotation axes intersecting near Leu 45. The four monomers are colored in yellow, blue, dark purple and light purple. ***a***, Top view looking down the flat surface of helix bundles in dimers. ***b***, Side view showing dimer–dimer stacking.

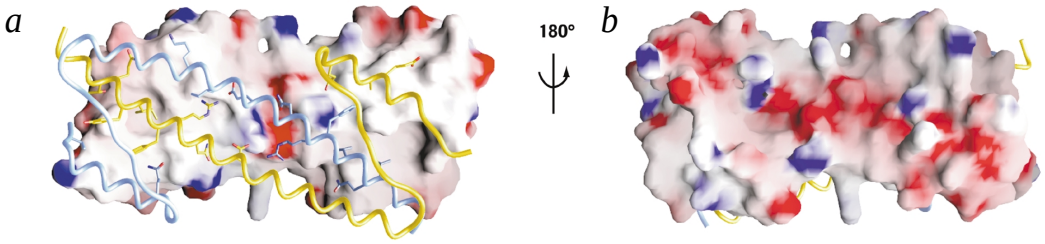

Fig. 4 Dimer–dimer interface. Upon the association of two dimers, ~3,400 Å^2 of the solvent-accessible surface is buried. There are two views of the surface electrostatic potential of one dimer, with the other dimer displayed as a ribbon. Basic regions on the surface are blue, and acidic regions are red. The side chains of the residues involved in dimer–dimer interactions are shown. ***a***, Front view of the highly hydrophobic surface involved in the association with another dimer. ***b***, Back view showing the highly hydrophilic surface that is solvent exposed.

Oligomerization domain as a drug target

The Bcr-Abl oligomerization domain has been shown to inhibit full-length Bcr-Abl oligomerization in a dominant-negative manner. The N-terminal 160 amino acids of Bcr, which contain the oligomerization domain as well as the full-length Bcr, inhibit Bcr-Abl transformation[16,17]. Because both the kinase and oligomerization domains are essential for Bcr-Abl oncogenicity, they may independently serve as drug targets. A specific kinase inhibitor has been shown to target the Abl kinase domain[18] and has been clinically effective in the treatment of CML[19]. However, drug-resistant leukemic cells have been observed in CML patients following drug treatment[20]. Targeting the BCR oligomerization domain may provide a complementary therapeutic approach to specifically disrupting Bcr-Abl transformation potential. Our crystal structure provides a template for the rational design of inhibitors disrupting Bcr-Abl oligomerization. There are several examples in the literature of identification of small molecules[21] or peptides that inhibit protein–protein interactions (including oligomerization). Inhibition of HIV-1 gp41 fusion protein with various peptides provides a clear proof-of-concept[22,23]. Our structure reveals that regular coiled-coil packing is key to dimerization of Bcr-Abl. Coiled coils are one of the best-studied (if not the best studied) protein–protein interface motifs, and it is reasonable to expect that future work will lead to the design and discovery of heterodimeric partner peptides to disrupt the homodimerization of Bcr-Abl.

Methods

Protein expression and purification. Using optimal codons for *Escherichia coli* expression[24], a synthetic gene sequence, denoted *Bcr*$_{1–74}$, was constructed to encode residues 1–74 of the human *Bcr* gene (SWISS-PROT: P11274). A Factor Xa cleavage site was incorporated upstream of the coding sequence. The constructed gene was inserted into the *Bam*HI–*Hin*dIII restriction sites of the expression vector pMALc2x (New England Biolabs), from which Bcr$_{1–74}$ can be expressed as a chimera with *E. coli* maltose binding protein (MBP). The plasmid pMBP/Bcr$_{1–74}$ was expressed in *E. coli* TOP 10 F′ competent cells. Cells were lysed by French press, and the fusion protein was purified using amylose agarose (New England Biolabs). Beads were suspended in Factor Xa cleavage buffer (50 mM Tris-HCl, pH 8.0, 100 mM NaCl and 2 mM $CaCl_2$). Factor Xa was added at a 1:500 (w/w) ratio of protease to fusion protein, and the reaction was incubated for 2 d at room temperature. During cleavage, approximately half of the Bcr$_{1–74}$ protein was further trimmed to Bcr$_{1–72}$. The two fragments, Bcr$_{1–74}$ and Bcr$_{1–72}$, were readily separated by reverse-phase high-performance liquid chromatography (HPLC) (Waters, Inc.) using a Vydac C18 preparative column (Vydac) with a water-acetonitrile gradient of 0.1% min^{-1} in the presence of 0.1% (v/v) trifluoroacetic acid. Peak fractions were verified by mass spectrometry and lyophilized. Bcr$_{30–65}$ was synthesized on a Perkin Elmer Model 431A peptide synthesizer using the method described[25]. All peptides had an acetylated N-terminus and a C-terminal amide. Peptides were purified by reverse-phase HPLC and lyophilized.

A *Bcr*$_{1–74}$*C38A* mutant gene fragment (Cys 38 mutated to Ala) was constructed by primer-mediated recombinant PCR mutagenesis[26]. The PCR product was inserted into the MBP-expression vector pMALc2x. pMBP/Bcr$_{1–74}$C38A plasmids were transformed into *E. coli* JM109 competent cells for protein expression. The purification scheme for the mutant protein was the same as for wild type. In the final step, two fragments — Bcr$_{1–74}$C38A and Bcr$_{1–72}$C38A — were purified and lyophilized. For SeMet protein expression, the pMBP/Bcr$_{1–74}$C38A vector and LacI^q gene-carrying pREP4 plasmids were cotransformed into *E. coli* strain DL41 (ref. 27). Large-scale cell growth was carried out as described[28]. SeMet-protein was purified by a procedure similar to that of the native protein, except 10 mM dithiothreitol (DTT) or β-mecaptoethanol was added to each digestion and purification step.

Table 1 Data collection, phasing, and refinement statistics

	SeMet λ1	SeMet λ2	SeMet λ3
Data collection (20.0–2.2 Å)			
Wavelength (Å)	0.9793	0.9789	0.9684
Completeness[1] (%)	99.2 (98.7)	99.5 (99.0)	99.3 (98.7)
R_{sym}[1,2]	0.054 (0.199)	0.060 (0.256)	0.062 (0.267)
Phasing statistics (20.0–2.6 Å)			
R_{cullis}[3]			
Acentric		0.85	0.85
Centric		0.90	0.67
Anomalous		0.62	0.67
Phasing power[4]			
(acentric / centric)		0.91 / 0.58	1.59 / 1.12
Overall figure of merit (before solvent flattening)			0.62

Refinement statistics (20.0–2.2 Å)	
Nonhydrogen protein atoms	4,366
Water molecules	422
Number of reflections	
Working	48,746
Test	2,505
R_{cryst}[1,5]	0.262(0.308)
R_{free}[1,5]	0.295(0.387)
R.m.s. deviations from ideal	
Bond lengths (Å)	0.008
Angles (°)	1.42

[1]Values in parentheses correspond to highest resolution shell (2.15–2.20 Å).
[2]$R_{sym} = \Sigma\Sigma_j|I_j - \langle I\rangle| / \Sigma\Sigma\,|\langle I\rangle|$, where I_j is the recorded intensity of the reflection j and $\langle I\rangle$ is the mean recorded intensity over multiple recordings.
[3]$R_{cullis} = \Sigma||F_{(\lambda i)} \pm F_{(\lambda 1)}| - |F_{h(\lambda i),c}|| / \Sigma\,|F_{(\lambda i)} \pm F_{(\lambda 1)}|$, where $F_{h(\lambda i),c}$ is the calculated heavy atom structure factor.
[4]Phasing power = $\langle F_{h(\lambda i)}\rangle$ / E, where $\langle F_{h(\lambda i)}\rangle$ is the r.m.s. heavy atom structure factor and E is the residual lack-of-closure error.
[5]R_{cryst}, $R_{free} = \Sigma||F_o| - |F_c|| / |F|$, where the crystallographic R-factor and R_{free} are calculated using the working and free reflection sets, respectively.

Circular dichroism (CD). CD experiments were performed on an Aviv 62A DS CD spectrometer. Measurements from 200–260 nm were performed in a 10 μM solution of protein sample in PBS (50 mM Na phosphate and 150 mM NaCl, pH 7.4) in a 1 mm pathlength cuvette. Thermal denaturation was performed in a 10 mm pathlength cuvette, and samples were heated from 0–98 °C, with equilibration times of 2 min and an averaging time of 1 min. Protein concentrations were determined by absorbance at 280 nm in 20 mM phosphate-buffered 6 M guanidine hydrochloride, pH 6.5 (ref. 29).

Crystallization, X-ray data collection and structure determination. The best-diffracting crystals grew from 1 μl of 10 mg ml^{-1} $Bcr_{1–72}$C38A sample added to 1 μl of reservoir buffer, containing ~2.5 M ammonium sulfate, and allowed to equilibrate against 500 μl of reservoir buffer. Crystals were in space group $P2_1$ (a = 36.31 Å, b = 122.12 Å, c = 60.45 Å, α = γ = 90° and β = 93.24°). SeMet-$Bcr_{1–72}$C38A was crystallized in ~1.8 M ammonium sulfate, and crystals were isomorphous to wild type protein. Prior to data collection, native and SeMet-$Bcr_{1–72}$C38A crystals were transferred into paraffin oil and flash-frozen using X-stream (Molecular Structure Corporation) or Oxford Cryosystems cryogenic crystal coolers. Initial data were collected on a Rigaku RU300 rotating-anode X-ray generator mounted on an R-axis IV area detector (Molecular Structure Corporation). Final native and MAD data sets for $Bcr_{1–72}$ were collected at the Howard Hughes Medical Institute Beamline X4A at Brookhaven National Laboratory using an ADSC Quantum-IV detector. For MAD data, the peak and inflection wavelengths of the selenium K absorption edge as well as the remote wavelength were selected based on the fluorescence spectrum of the SeMet-$Bcr_{1–72}$ crystal (Table 1). To minimize crystal decay between data sets, they were collected in 20° batches, allowing each batch to be collected at each wavelength before moving on to the next. Reflections were integrated and scaled with DENZO and SCALEPACK[30]. Further diffraction data processing, phase determination and map calculations were performed using the CCP4 suite[31]. Intensities were reduced to amplitudes with TRUNCATE[31], and the data sets for the wavelengths closest to the selenium K absorption edge (λ1, λ2) were scaled with SCALEIT[31] to the remote wavelength (λ3) data set (Table 1). MAD phases were generated with MLPHARE[31] (Table 1) from 20 selenium atoms located within the asymmetric unit using SOLVE[32]. Phases were improved and extended to higher resolution with DM[33]. Electron density map interpretation and model building were done with O[34]. The structure of $Bcr_{1–72}$ was refined at 2.2 resolution using CNS[35]. Both native and MAD data were persistently affected by crystal freezing. For final refinement, we used the MAD (λ1) data because it suffered less from freezing artifacts and yielded better statistics. The correctness of the structure was checked with simulated annealing omit maps and with PROCHECK[36]. All residues of $Bcr_{1–72}$ occupy the favored areas of the Ramachandran plot. The conformations of the majority of the residues are well defined, except for a few terminal residues and the loop regions between α-helices.

Coordinates. The coordinates for $Bcr_{1–72}$ have been deposited in the Protein Data Bank (accession code 1K1F) and are available immediately at the website *http://web.wi.mit.edu/kim*.

Acknowledgments

We thank J. Pang and C. Kitidis for technical assistance; L. Gaffney for assistance in preparation of the manuscript; B. Chen, S. Johnston, A. Keating, C. Liu, J. Marszalek, J. Newman, R. Ren and M. Root for comments on manuscript; and C. Ogata for assistance at the Howard Hughes Medical Institute beamline (X4A) at the National Synchrotron Light Source (Brookhaven National Laboratory, Upton, NY). This research was funded by the National Institutes of Health and National Science Foundation, and utilized the W. M. Keck Foundation X-ray Crystallography Facility (Whitehead Institute, Cambridge, MA). X.Z. was supported by an Anna Fuller fellowship, and S.G. was supported by a Clinician Scientist Award from the NIH.

Correspondence should be addressed to P.S.K. *email: peter_kim@merck.com*

Received 16 August, 2001; accepted 20 November, 2001.

1. Gotoh, A. & Broxmeyer, H.E. *Curr. Opin. Hematol.* **4**, 3–11 (1997).
2. Sawyers, C.L. *N. Engl. J. Med.* **340**, 1330–1340 (1999).
3. Ponticelli, A.S., Whitlock, C.A., Rosenberg, N. & Witte, O.N. *Cell* **29**, 953–960 (1982).
4. Pendergast, A.M., Muller, A.J., Havlik, M.H., Maru, Y. & Witte, O.N. *Cell* **66**, 161–171 (1991).
5. McWhirter, J.R. & Wang, J.Y. *Mol. Cell. Biol.* **11**, 1553–1565 (1991).
6. McWhirter, J.R., Galasso, D.L. & Wang, J.Y. *Mol. Cell. Biol.* **13**, 7587–7595 (1993).
7. Hendrickson, W.A. *Science* **254**, 51–58 (1991).
8. Pendergast, A.M., Clark, R., Kawasaki, E.S., McCormick, F.P. & Witte, O.N. *Oncogene* **4**, 759–766 (1989).
9. Bennett, M.J., Schlunegger, M.P. & Eisenberg, D. *Protein Sci.* **4**, 2455–2468 (1995).
10. Crick, F.H.C. *Acta Crystallogr.* **6**, 689–697 (1953).
11. O'Shea, E.K., Klemm, J.D., Kim, P.S. & Alber, T. *Science* **254**, 539–544 (1991).
12. Cohen, C. & Parry, D.A. *Science* **263**, 488–489 (1994).
13. McWhirter, J.R. & Wang, J.Y. *Oncogene* **15**, 1625–1634 (1997).
14. Papadopoulos, P., Ridge, S.A., Boucher, C.A., Stocking, C. & Wiedemann, L.M. *Cancer Res.* **55**, 34–38 (1995).
15. Schlessinger, J. *Cell* **103**, 211–225 (2000).
16. Guo, X.Y. *et al. Oncogene* **17**, 825–833 (1998).
17. Wu, Y. *et al. Oncogene* **18**, 4416–4424 (1999).
18. Schindler, T. *et al. Science* **289**, 1938–1942 (2000).
19. Mauro, M.J. & Druker, B.J. *Curr. Oncol. Rep.* **3**, 223–227 (2001).
20. Gorre, M.E. *et al. Science* **293**, 2163 (2001).
21. Degterev, A. *et al. Nature Cell Biol.* **3**, 173–182 (2001).
22. Chan, D.C. & Kim, P.S. *Cell* **93**, 681–684 (1998).
23. Eckert, D.M. & Kim, P.S. *Annu. Rev. Biochem.* **70**, 777–810 (2001).
24. Makrides, S.C. *Microbiol. Rev.* **60**, 512–538 (1996).
25. Lockhart, D.J. & Kim, P.S. *Science* **257**, 947–951 (1992).
26. Higuchi, R., Krummel, B. & Saiki, R.K. *Nucleic Acids Res.* **16**, 7351–7367 (1988).
27. Hendrickson, W.A., Horton, J.R. & LeMaster, D.M. *EMBO J.* **9**, 1665–1672 (1990).
28. Yang, W., Hendrickson, W.A., Kalman, E.T. & Crouch, R.J. *J. Biol. Chem.* **265**, 13553–13559 (1990).
29. Edelhoch, H. *Biochemistry* **6**, 1948–1954 (1967).
30. Otwinowski, Z. In *Data collection and processing* (ed. Sawer, L., Isaacs, N. & Bailey, S.) 55–62 (SERC, Daresbury Laboratory, Warrington; 1993).
31. Collaborative Computational Project, Number 4. *Acta Crystallogr. D* **50**, 760–763 (1994).
32. Terwilliger, T.C. & Berendzen, J. *Acta Crystallogr. D* **55**, 849–861 (1999).
33. Cowtan, K. & Main, P. *Acta Crystallogr. D* **54**, 487–493 (1998).
34. Jones, T.A., Zou, J.W., Cowan, S. & Kjeldgaard, M. *Acta Crystallogr. D* **47**, 110–119 (1991).
35. Brünger, A.T. *et al. Acta Crystallogr. D* **54**, 905–921 (1998).
36. Laskowski, R.A., MacArthur, M.W., Moss, D.S. & Thornton, J.M. *J. Appl. Crystallogr.* **26**, 283–291 (1993).
37. Verfaillie, C.M. *Hematol. Oncol. Clin. North Am.* **12**, 1–29 (1998).
38. McLachlan, A.D., Stewart, M. & Smillie, L.B. *J. Mol. Biol.* **98**, 281–291 (1975).
39. Lupas, A., Van Dyke, M. & Stock, J. *Science* **252**, 1162–1164 (1991).
40. Berger, B. *et al. Proc. Natl. Acad. Sci. USA* **92**, 8259–8263 (1995).
41. Kraulis, P.J. *J. Appl. Crystallogr.* **24**, 946–950 (1991).
42. Nicholls, A., Sharp, K.A. & Honig, B. *Proteins* **11**, 281–296 (1991).